



Molybdenum containing cage like mesoporous KIT-5 for enhanced catalytic conversion of 1-butene and ethylene to propene

Kai Tao^a, Qingxiang Ma^d, Noritatsu Tsubaki^c, Shenghu Zhou^{b,*}, Lei Han^{a,*}

^a Institute of Inorganic Materials, School of Materials Science & Chemical Engineering, Ningbo University, Ningbo, Zhejiang 315211, China

^b School of Chemical Engineering, East China University of Science and Technology, Shanghai 200237, China

^c Department of Applied Chemistry, School of Engineering, University of Toyama, Gofuku 3190, Toyama 930-8555, Japan

^d State Key Laboratory Cultivation Base of Natural Gas Conversion, College of Chemistry & Chemical Engineering, Ningxia University, Yinchuan 750021, China



ARTICLE INFO

Article history:

Received 22 January 2016

Received in revised form 18 February 2016

Accepted 18 February 2016

Available online 22 February 2016

Keywords:

Mo-KIT-5

Mesoporous

Isomerization

Metathesis

Propene

ABSTRACT

Molybdenum containing three-dimensional (3D) cage-like mesoporous KIT-5 (Mo-KIT-5) materials with various Si/Mo ratios was successfully prepared by one-pot hydrothermal synthesis. The obtained materials were characterized by various techniques, such as XRD, N₂ physisorption, TEM, FTIR, UV-DRS, XPS, and NH₃-TPD. Characterization results revealed that molybdenum species could be finely dispersed in the framework of KIT-5 without disturbing long-range ordering at Si/Mo ratios higher than 15, while collapse of mesoporous structure and presence of bulk MoO₃ was observed for Mo-KIT-5 sample with a Si/Mo ratio of 5. Mo-contained materials were investigated in catalytic conversion of 1-butene and ethylene to propene. Among all of Mo-KIT-5 materials studied, Mo-KIT-5-40 with Si/Mo ratio of 40 exhibited best catalytic performance caused by the fact that it processed superior textural properties, substantial active Mo species, and appropriate amount of acidic sites. Further decreasing the Si/Mo ratio resulted in declined activity due to the presence of extraframework Mo species. It was found that doped Mo-KIT-5-40 showed better catalytic activity than control supported Mo/KIT-5-40 and Mo/SiO₂-40 catalysts with same Mo loading due to the highly dispersed active Mo species on the mesoporous framework. Moreover, Mo-KIT-5 was also superior to other Mo containing mesoporous materials, such as Mo-SBA-15 with two-dimensional pores and Mo-KIT-6 with three-dimensional cylindrical pores, implying the advantage of this kind of ordered 3D cage-like mesoporous materials in this reaction.

© 2016 Elsevier B.V. All rights reserved.

1. Introduction

Propene is a highly demanded basic building block in petrochemical industry, which is mainly obtained through steam cracking of oil based feedstocks, such as ethane, naphtha and gas oils. Alternatively, methanol to propene (MTP) or methanol to olefins (MTO) producing propene from non-oil resources has attracted great attentions [1]. However, a considerable amount of butene is generated as byproduct. Olefin metathesis, which can convert C4 byproducts into valuable propene, providing an efficient way of utilizing C4 and increasing the yield of propene, is of great importance for industrial application [2]. Since the first report of olefin metathesis in 1964 [3], many supported metathesis catalysts have been developed, including rhenium [4], tungsten [5] and

molybdenum [6] based catalysts. Re based catalysts exhibited outstanding catalytic performance for metathesis. But, the high price and limited availability restricts the application of Re. Alternatively, W and Mo with lower cost and compatible catalytic performance were extensively explored for metathesis of olefin.

The performance of supported metathesis catalyst was profoundly influenced by the nature of supports [7,8], such as textural properties and acidity. The most widely used supports were conventional SiO₂ [9], Al₂O₃ [10], zeolite [11] and mixed metal oxide [12]. The rapid development of mesoporous materials during the last decades has stimulated the exploration of mesoporous molecular sieves (MMS) and organized mesoporous alumina (OMA) as metathesis catalysts [13]. Mesoporous materials possessing uniform mesopores, large surface area and pore volume, compared with conventional supports. The large surface area could afford a high amount of active sites and the uniform mesopores facilitate the intra-pore diffusion of reactants and products. To date, many MMS such as MCM-41 [7,14], MCM-48 [7], SBA-15 [7,14–16], HMS [17],

* Corresponding authors.

E-mail addresses: zhoushenghu@ecust.edu.cn (S. Zhou), hanlei@nbu.edu.cn (L. Han).

and KIT-6 [18] have been employed as the supports of metathesis catalysts. In brief, MMS supported W (Mo) catalysts exhibited better catalytic performance than that of conventional silica gels supported catalysts due to the better dispersion of active species on MMS. In addition, the pore size and architecture of MMS also influenced the metathesis activity. Topka et al. [7] systematically studied the metathesis of 1-octene over three typical MMS, i.e. MCM-41, MCM-48, and SBA-15 supported Mo catalysts and the catalytic activity decreased in the order: MCM-41 > MCM-48 > SBA-15. The different dispersion of active species over three supports was responsible for the difference in catalytic performance. Bhuiyan et al. [14] also compared the catalytic property of W-SBA-15 and W-MCM-41 in 2-butene metathesis to propene, and found that W-MCM-41 catalyst showed better activity than that of W-SBA-15. The better activity of W-MCM-41 was attributed to the well-dispersed active tetrahedral tungsten oxide species. Besides mesoporous silica, mesoporous alumina [19] and alumina-silica [20,21] based catalysts also showed promising metathesis activity.

KIT-5, a novel mesoporous silica with ordered 3D cage-like mesopores was first reported by Kleitz et al. [22]. KIT-5 was believed to be superior to 1D mesoporous silicas, because the interconnected 3D large pores were beneficial for mass transportation of reactants and products, and providing more accessible adsorption sites [23]. Therefore, KIT-5 was a desirable catalyst supports for versatile reactions [24–26]. Herein we first report the synthesis of high active mesoporous Mo-KIT-5 catalyst for production of propene from metathesis of 1-butene and ethylene. The catalyst was systematically characterized by multiple characterization techniques. The Mo-KIT-5-40 catalyst exhibited an improved catalytic performance compared with control supported Mo/KIT-5-40 and Mo/SiO₂-40 catalysts with same Mo loading due to high dispersion of active Mo species. The Mo-KIT-5 catalyst was also advantageous to other mesoporous catalysts, such as Mo-SBA-15 and Mo-KIT-6.

2. Experimental

2.1. Chemicals

Pluronic F127 ($M_w = 12,500$) was purchased from Sigma-Aldrich as the structure directing agent. Tetraethyl orthosilicate (TEOS, AR) and ammonium paramolybdate ($(\text{NH}_4)_6\text{Mo}_7\text{O}_{24} \cdot 4\text{H}_2\text{O}$, AR) were purchased from Sinopharm Chemical Reagent Co., Ltd., as silicon and Mo sources, respectively. Silica gel (BET surface area, 399 m²/g) was obtained from Qingdao Haiyang Chemical Co., Ltd. All the reagents were used as received without further purification.

2.2. Catalyst preparation

2.2.1. Synthesis of Mo-KIT-5 catalysts

The Mo-KIT-5 catalysts with various Si/Mo were prepared using Pluronic F127 as the structure directing agent following the procedure described by Kleitz et al. [22]. Typically, 4 g F127 and required amount of ammonium paramolybdate were dissolved in 192 g deionized water and 8.4 g of 35 wt% hydrochloric acid under stirring. To this mixture, 19.2 g of TEOS was dropwise added. The resulting mixture was vigorously stirred at 45 °C for 24 h. Then, the mixture was transferred to a Teflon-lined autoclave, and subject to a hydrothermal treatment at 100 °C for 24 h. The products were collected by filtering without washing, and drying at 100 °C overnight. Finally, the removal of F127 templates was achieved by calcining the sample in a muffle oven at 550 °C for 4 h with a heating rate of 1 °C/min. The catalyst was denoted as Mo-KIT-5-x, where the x represented the Si/Mo ratio in the synthesis gel.

Pure KIT-5 was prepared using the same procedure as Mo-KIT-5 samples except without adding of ammonium paramolybdate.

2.2.2. Preparation of control Mo/KIT-5-40 and Mo/SiO₂-40 catalysts

For comparison, KIT-5 and SiO₂ supported Mo catalysts were synthesized by wet-impregnation of traditional SiO₂ gel and KIT-5 with 10 ml of ammonium paramolybdate aqueous solution. The impregnated sample was dried at 110 °C overnight and calcined at 550 °C for 4 h with a ramping rate of 1 °C/min. The Mo loading of both catalysts were fixed at 2.5 wt%, which was identical to that of Mo-KIT-5-40, as confirmed by inductively coupled plasma optical emission spectroscopy (ICP-OES). The catalysts were denoted as Mo/KIT-5-40 and Mo/SiO₂-40, respectively, where 40 was the nominal Si/Mo ratio.

2.3. Catalyst characterization

Inductively coupled plasma optical emission spectroscopy (ICP-OES) analysis was employed to determine the real Mo content of sample using PerkinElmer OPTIMA 2100 DV optical emission spectrometer. Small-angle X-ray diffraction (SAXD) and wide-angle X-ray diffraction (WAXD) patterns of samples were collected on a Bruker AXS D8 Advance diffractometer with Cu K α radiation in the 2 θ angle range of 0.5–5° and 20–80°, respectively. N₂ adsorption–desorption isotherm of the sample was measured at 77 K using a Micrometrics ASAP-2020M adsorption apparatus. Before the measurement, the sample was outgassed at 200 °C for 6 h. The specific surface area was determined by the multiple Brunauer–Emmett–Teller (BET) method. The pore volume and pore size distribution were obtained from the adsorption branch of the isotherm using Barrett–Joyner–Halenda (BJH) method. Transmission electron microscopy (TEM) images were acquired on a JEOL 2100 transmission electron microscope operated at 200 kV. The Fourier transform infrared spectra (FTIR) were recorded with a Bruker Tensor 27 spectrophotometer. UV-vis diffuse reflectance spectra (UV-DRS) were performed in PE Lambda 950 equipment using BaSO₄ as reference. X-ray photoelectron spectroscopy (XPS) studies were performed on AXIS ULTRA DLD multifunctional X-ray photoelectron spectroscopy with an Al source. Temperature programmed desorption of ammonia (NH₃-TPD) was carried out in a quartz micro-reactor. 0.1 g catalyst was pretreated at 550 °C for 30 min in He (25 cm³ min⁻¹) prior to NH₃-TPD measurement before the reactor was cooled down to room temperature, and then the sample was saturated with NH₃. The physically absorbed NH₃ was removed by flushing the sample with He at 120 °C for 2 h. Temperature-programmed desorption of ammonia was carried out from 120 to 650 °C with a ramping rate of 5 °C/min, and the amount of desorbed NH₃ was monitored by a thermal conductivity detector (TCD).

2.4. Metathesis reactions

Catalytic performance of as-synthesized catalysts for metathesis of 1-butene and ethylene to propene was evaluated in a fixed-bed stainless reactor (i.d. 10 mm) under atmospheric pressure. In each test, 1 g of shaped catalyst (20–40 mesh) was placed at the center of the reactor and sandwiched by inert SiO₂ beads. Prior to reaction, the catalysts were in situ activated by high pure N₂ (35 ml/min) at 550 °C for 4 h to remove the moisture, followed by cooling down to reaction temperature. Then, a mixture of ethylene and 1-butene ($n\text{C}_2\text{H}_4/n\text{C}_4\text{H}_8 = 2$) was introduced and the reaction was started. The metathesis reaction conditions were 450 °C, 0.1 MPa, weight hourly space velocity (WHSV, 1-C₄H₈ + C₂H₄) of 0.8 h⁻¹. The effluent gases released from the reactor were analyzed by an online gas chromatograph (GC) equipped with a flame ionization detector (FID). The calculation of 1-butene conversion and product selectivity has been described elsewhere [15,18].

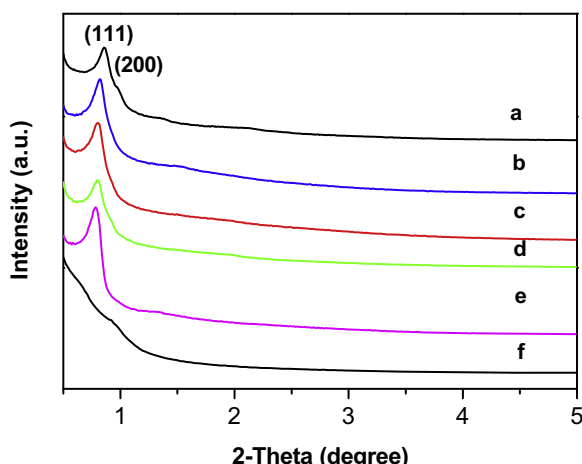


Fig. 1. Small-angle XRD patterns of pure KIT-5 (a) and Mo containing KIT-5 samples: (b) Mo-KIT-5-60, (c) Mo-KIT-5-40, (d) Mo-KIT-5-25, (e) Mo-KIT-5-15 and (f) Mo-KIT-5-5.

Table 1
Textural properties of KIT-5 and Mo containing catalysts.

Sample	a_0 (nm) ^a	BET surface area ($\text{m}^2 \text{g}^{-1}$)	Pore volume ($\text{cm}^3 \text{g}^{-1}$)	Pore size (nm)
KIT-5	17.8	636.2	0.29	3.5
Mo-KIT-5-60	18.8	831.1	0.55	3.9
Mo-KIT-5-40	19.0	814.4	0.55	4
Mo-KIT-5-25	19.3	700.1	0.54	3.9
Mo-KIT-5-15	19.6	653.7	0.52	3.9
Mo-KIT-5-5	—	144.9	0.49	12.6
Mo/KIT-5-40	—	458.2	0.22	1.8
Mo/SiO ₂ -40	—	355.6	0.81	9.2

^a Unit cell parameter (a_0) was determined by the formula: $a_0 = d_{111} \sqrt{3}$.

3. Results and discussion

3.1. Characterization of catalysts

In present study, Mo containing KIT-5 catalysts (Mo-KIT-5) with various Si/Mo ratios were prepared by one pot hydrothermal synthesis from ammonium paramolybdate and TEOS in presence of F127 under acidic condition. The real Si/Mo ratios in the final catalysts were checked by ICP-OES. The result is presented in Table S1. For all Mo-KIT-5 samples, the real Si/Mo ratios were higher than those in the synthesis solution, as similar to the case of W-KIT-5 [27]. This could be explained by the fact that the Mo species tended to be in cationic rather than oxo forms in an acidic medium.

Small-angle X-ray diffraction (SAXD) is an efficient tool to study the ordered mesoporous materials. The SAXD patterns of KIT-5 and Mo-KIT-5 catalysts are shown in Fig. 1. Two resolved diffraction peaks in the 2θ range of $0.5\text{--}1.0^\circ$ indexed to (111) and (200) plane was observed for pristine KIT-5, which were characteristics of face centered close-packed cubic type materials with $Fm\bar{3}m$ space group symmetry [22]. Compared with pure KIT-5, Mo-KIT-5 with a higher Si/Mo ratio showed more intense (111) diffraction peak. This revealed that the incorporation of an appropriate amount of Mo were helpful for retain of the mesoporous structure. However at a very low Si/Mo ratio (Mo-KIT-5-5), no resolved reflections are found, which suggested that the long-range ordering was lost when excessive Mo was involved. The unit cell parameters (a_0) were calculated from d_{111} and presented in Table 1, which were similar to those of previously reported KIT-5 type materials [28]. The unit cell parameter increased with Mo loading. This could be attributed to the incorporation of Mo in the KIT-5 framework, since the atomic radius of Mo is larger than that of Si⁴⁺.

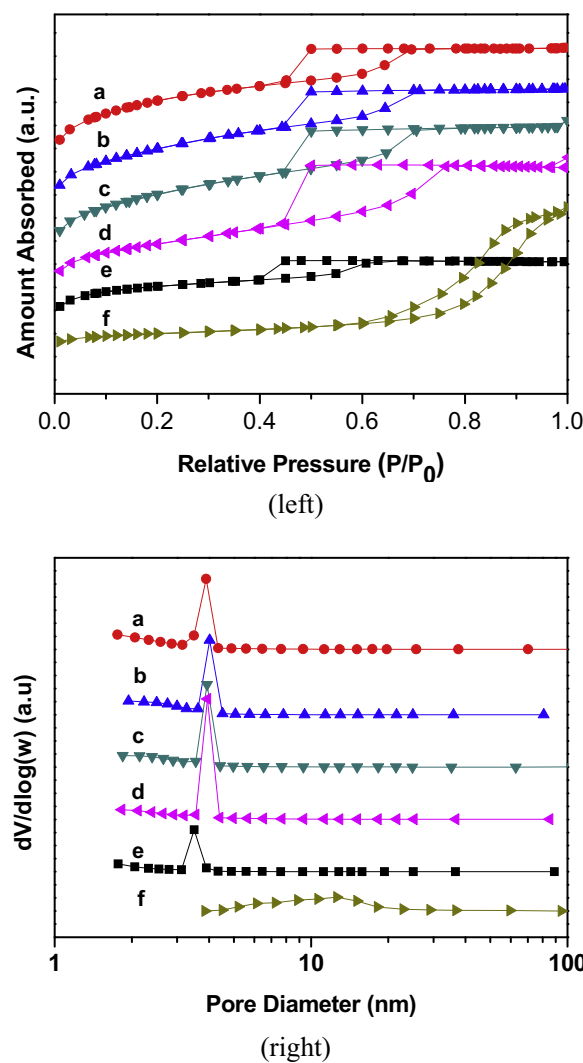


Fig. 2. N₂ adsorption–desorption isotherms (left) and pore size distributions (right) of various samples: (a) Mo-KIT-5-60, (b) Mo-KIT-5-40, (c) Mo-KIT-5-25, (d) Mo-KIT-5-15, (e) KIT-5 and (f) Mo-KIT-5-5.

The porosity of samples is studied by N₂ physisorption at -196°C . The N₂ adsorption–desorption isotherms and pore size distributions of pure KIT-5 and Mo-KIT-5 catalysts are shown in Fig. 2. KIT-5 showed type IV isotherm with a sharp capillary condensation and a broad H2-type hysteresis loop, indicating that the material were ordered mesoporous and possessed large uniform cage-like pores [22]. KIT-5 displayed a narrow pore size distribution centered at 3.5 nm. Upon incorporating Mo, Mo-KIT-5 (Si/Mo = 60, 40, 25 and 15) catalysts showed similar isotherm profiles to that of pristine KIT-5 but with higher amount of N₂ adsorption and capillary condensation step. This phenomenon was also observed for Al-KIT-5 samples [29]. Besides, the capillary condensation was shifted to higher relative pressure with the concomitant increase of pore size. However, further increasing the Mo loading resulted in a dramatic change of isotherm as for Mo-KIT-5-5, which suggested that the ordered mesoporous structure was destroyed. The Mo-KIT-5-5 sample also showed a very broad pore size distribution.

The BET surface area, pore volume and mean pore size of catalysts are summarized in Table 1. The BET surface area and pore volume of pristine KIT-5 were $636.2 \text{ m}^2 \text{ g}^{-1}$ and $0.29 \text{ cm}^3 \text{ g}^{-1}$, respectively. Upon incorporation of Mo, Mo-KIT-5 catalysts showed larger BET surface area and pore volume compared with pure KIT-5 and the BET surface area decreased from 831.1 to $653.7 \text{ m}^2 \text{ g}^{-1}$

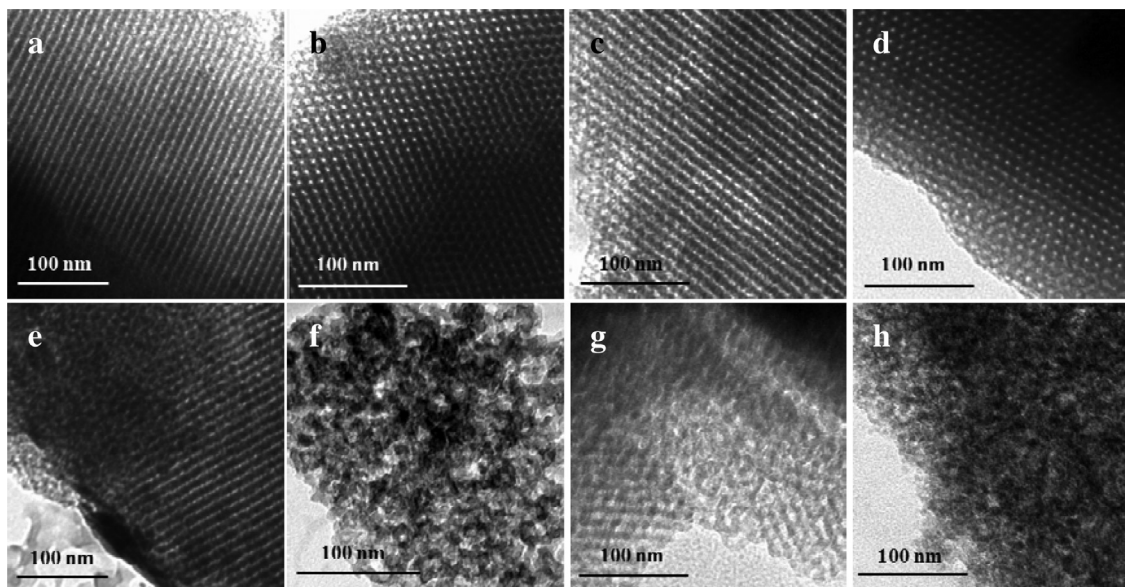


Fig. 3. TEM images showing (a) KIT-5, (b) Mo-KIT-5-60, (c) Mo-KIT-5-40, (d) Mo-KIT-5-25, (e) Mo-KIT-5-15, (f) Mo-KIT-5-5, (g) Mo/KIT-5-40 and (h) Mo/SiO₂-40.

with decreasing Si/Mo ratio from 60 to 15. For Mo-KIT-5-5, the BET surface area was as low as 144.9 m² g⁻¹, indicating the loss of mesoporous ordering. Compared with one-pot synthesized Mo-KIT-5-40, supported Mo/KIT-5-40 showed lower BET surface area, and smaller pore volume and pore size. This was caused by the plugging of partial mesopores by Mo species during the impregnation process [30].

The morphology of materials was observed directly by TEM. TEM images of various samples are provided in Fig. 3. As shown in Fig. 3a, pristine KIT-5 sample displayed a cubic three-dimensional ordered mesoporous structure similar to those reported by other authors [22,27]. After the introduction of Mo, Mo-KIT-5-60 (Fig. 3b), Mo-KIT-5-40 (Fig. 3c), Mo-KIT-25 (Fig. 3d) and Mo-KIT-15 (Fig. 3e) samples also showed mesoporous structures with long-range ordering. In a sharp contrast, the mesoporous structure disappeared and some bulk agglomerate appeared for KIT-5-5 as clearly shown in Fig. 3f. The results suggested that mesoporous structure of KIT-5 could be reserved after doping Mo with Si/Mo ratio as low as 15, and too excessive Mo involved resulted in the collapse of mesoporous structure, as also suggested by N₂ physisorption result. Supported Mo/KIT-5-40 also showed well mesoporous structure except some disordered region compared with Mo-KIT-5-40. Mo/SiO₂-40 displayed a typical morphology of amorphous SiO₂ with indiscernible nano particles [15].

The crystalline phases of Mo-containing catalysts were studied by wide-angle powder X-ray diffraction. XRD patterns of various samples are shown in Fig. 4. Only a broad diffraction peak centered in the 2θ range of 15–30° were found for one-pot synthesized Mo-KIT-5 catalyst with Si/Mo ratio ranged from 15 to 60, which was characteristic of amorphous silica. No characteristic peaks corresponding to MoO₃ could be observed, suggesting that the Mo species were well dispersed in the KIT-5 framework. Further increasing the loading of Mo, intense diffraction peaks ascribed to MoO₃ obviously appeared, indicating the formation of extraframework MoO₃ species. Ramanathan et al. [27] found that extraframework WO₃ phase was formed at very high Si/W ratio (100). In this work, no MoO₃ was found at Si/Mo ratio as low as 15, suggesting high dispersion of Mo species in the KIT-5 framework or formation of amorphous MoO₃. The supported Mo/KIT-5-40 showed similar diffraction patterns to that of one-step synthesized Mo-KIT-5-40 catalyst. For conventional Mo/SiO₂-40, the presence of nanosized MoO₃ species is confirmed by the weak diffraction

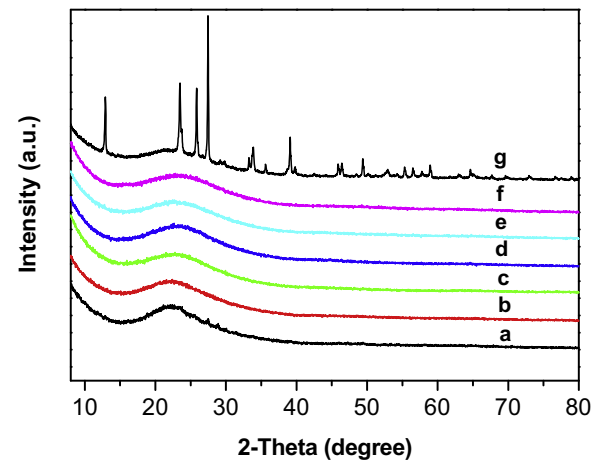


Fig. 4. Wide-angle XRD patterns of various Mo containing catalysts: (a) Mo/SiO₂-40, (b) Mo/KIT-5-40, (c) Mo-KIT-5-60, (d) Mo-KIT-5-40, (e) Mo-KIT-5-25, (f) Mo-KIT-5-15 and (g) Mo-KIT-5-5.

peaks in 20–30° 2θ range. XRD result indicated that the mesoporous catalyst exhibited higher Mo distribution than conventional catalyst, which could be ascribed to the superior textural properties of mesoporous materials as shown in Table 1.

The FTIR spectra of KIT-5 and Mo-containing catalysts are shown in Fig. 5. All samples displayed absorption bands around 465, 800, 1080, 1385, and 1636 cm⁻¹. The band at 465 cm⁻¹ corresponded to the internal deformation vibration of Si—O—Si bond [31]. The 800 and 1080 cm⁻¹ band were assigned to symmetric and asymmetric stretching of bulk Si—O—Si for the tetrahedral SiO₄⁴⁻ structure units, respectively [32]. The characteristic band of C—H deformation band of the methyl groups³² (relevant to residual organic group) or absorbed CO₂ [33] appeared at 1385 cm⁻¹. In this work, the 1385 cm⁻¹ band became very weak after Mo was introduced, indicating that this band was associated with absorbed CO₂, since the acidity generated by Mo incorporation (see NH₃-TPD result) will reduce the absorption of CO₂. The 1636 cm⁻¹ band observed in all spectra can be indexed to water [31]. It should be noted that with the increase of Mo content, a new band at 908 cm⁻¹ became evident, which can be ascribed to the terminal Mo=O groups in

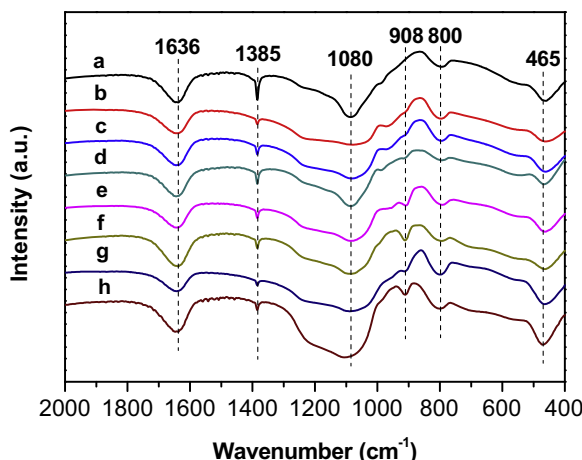


Fig. 5. FTIR spectra of various samples: (a) KIT-5, (b) Mo-KIT-5-60, (c) Mo-KIT-5-40, (d) Mo-KIT-5-25, (e) Mo-KIT-5-15, (f) Mo-KIT-5-5, (g) Mo/KIT-5-40 and (h) Mo/SiO₂-40.

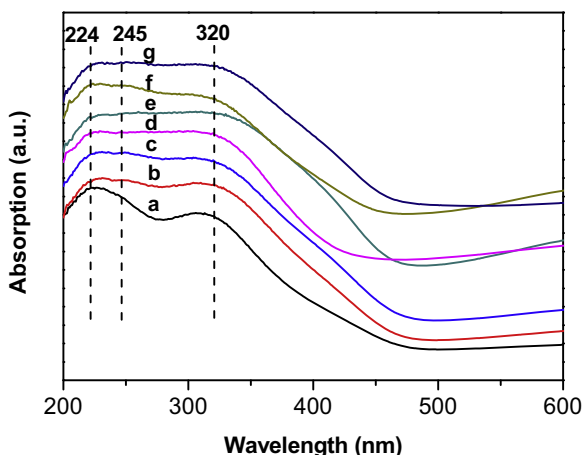


Fig. 6. Diffuse reflectance UV-vis spectra of various Mo-containing samples: (a), Mo-KIT-5-60, (b) Mo-KIT-5-40, (c) Mo-KIT-5-25, (d) Mo-KIT-5-15, (e) Mo-KIT-5-5, (f) Mo/KIT-5-40 and (g) Mo/SiO₂-40.

Mo—O—Si vibration [34], revealing that Mo was successfully incorporated into the silica matrix.

UV-vis diffuse reflectance spectra (UV-DRS) were performed to study the chemical state of Mo species, since UV-DRS was a very efficient in probing local molecular coordination of metal oxide in the framework and/or in the extra framework of mesoporous structure [35]. Fig. 6 shows the UV-DRS profiles of various Mo-containing samples. Pure KIT-5 showed no absorption bands (not shown here). Three absorption bands around 224, 245, and 320 nm were found for all Mo-containing samples. The bands around 220–250 nm were assigned to the tetrahedral molybdate species, whereas the band around 320 nm was ascribed to the octahedral coordinated Mo—O—Mo bridge bond [15,36]. A red-shift of 320 nm band and concomitant increase in intensity were observed for Mo-KIT-5 catalysts as Si/Mo ratio decreased and Mo-KIT-5-5 displayed a strong band beyond 320 nm, suggesting the generation of larger Mo species clusters as found by TEM (Fig. 3f).

XPS experiment was conducted to analyze the oxidation states of Mo species in Mo-KIT-5. Fig. 7 shows a representative Mo 3d spectrum of Mo-KIT-5-40 sample. The spectrum consists of two individual Mo 3d_{5/2} and Mo 3d_{3/2} doublets. Four deconvoluted components located at 231.6, 232.9, 234.7, and 236.1 eV were observed from the figure. Signals at 232.9 and 236.1 eV were assigned to Mo in a high oxidation state, namely, Mo⁶⁺ 3d_{5/2} and

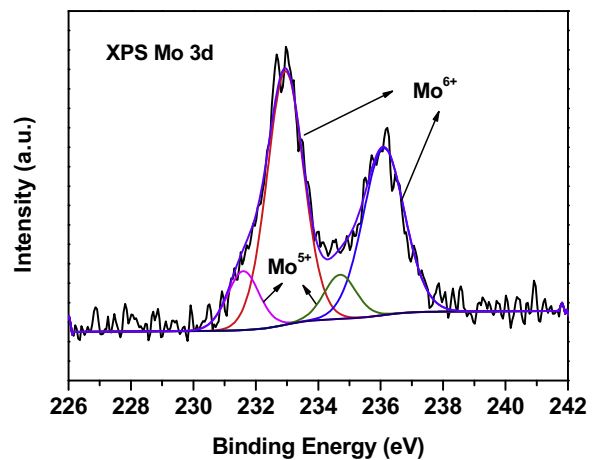


Fig. 7. XPS spectra of Mo-KIT-5-40 sample.

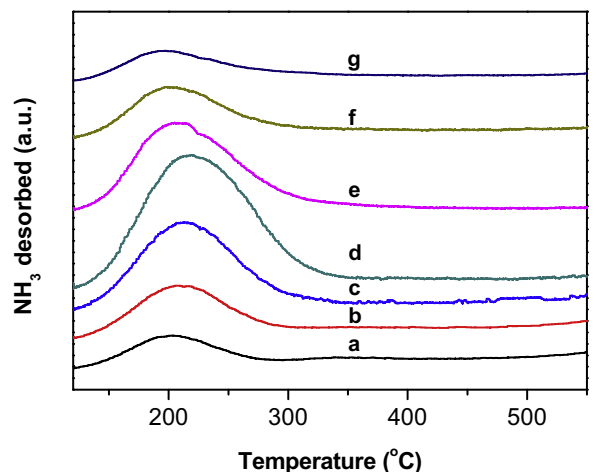
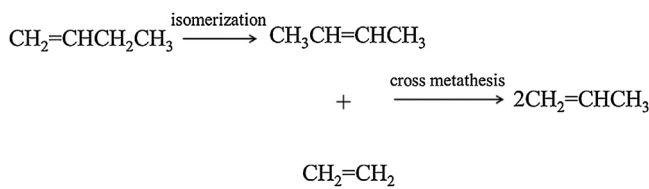


Fig. 8. NH₃-TPD curves of various Mo-containing catalysts: (a), Mo-KIT-5-60, (b) Mo-KIT-5-40, (c) Mo-KIT-5-25, (d) Mo-KIT-5-15, (e) Mo-KIT-5-5, (f) Mo/KIT-5-40 and (g) Mo/SiO₂-40.

Mo⁶⁺ 3d_{3/2}, respectively, while signals at 231.6 and 234.7 eV were ascribed to Mo⁵⁺ 3d_{5/2} and Mo⁵⁺ 3d_{3/2}, respectively [15]. XPS result revealed that the Mo-KIT-5 catalyst contained both Mo⁶⁺ and Mo⁵⁺ species. The presence of a portion of Mo⁵⁺ species was considered to be crucial for the catalytic activity of 1-butene metathesis [15].

NH₃-TPD experiments were carried out to survey the acidity of various samples. The NH₃-TPD profiles of Mo-containing catalysts are presented in Fig. 8. The negligible amount of NH₃ desorbed from pure KIT-5 (not shown here) was indicative of its neutral nature. However, all Mo-containing samples showed broad NH₃ desorption peaks in temperature range of 150 to 300 °C with peak maxima centered around 190–220 °C. Generally, the NH₃-TPD curve could be divided into two regions, namely low temperature (<400 °C) and high-temperature (>400 °C) regions. The former was assigned to the desorption of NH₃ from weak acid sites, and the later was attributed to the desorption of NH₃ from strong Brønsted and Lewis type acid sites [34]. In this work, no NH₃ desorption peaks could be found in the high-temperature zone. Thus, it was suggested that all Mo based catalysts contained only weak acid sites. For Mo-KIT-5 catalyst, the amount of acid initially increased with decreasing the Si/Mo ratio down to 15 and then declined when the Si/Mo was further decreased to 5, judging from the intensity of NH₃-TPD band as shown in Fig. 8a–e. The acidity of catalyst was derived from the coordinative unsaturated Mo⁶⁺ species on the surface [37] and the hydroxyl groups formed by protonating the bridging Si=O=Mo or



Scheme 1. The main reaction pathways of catalytic conversion of 1-butene and ethylene over Mo-KIT-5 catalysts.

terminal MoO bonds on the surface of the samples [38,39]. Therefore, the decrease of the acidity at low Si/Mo ratio (Mo-KIT-5-5) could be caused by the formation of bulk MoO_3 species, as confirmed by XRD (Fig. 4 g) and TEM (Fig. 3f). Besides, at the same content of Mo, mesoporous Mo-KIT-5-40 and Mo/KIT-5-40 catalysts exhibited more acidic sites than conventional Mo/SiO₂-40 catalyst.

3.2. Catalytic activity

Various Mo-containing catalysts were tested in catalytic conversion of 1-butene and ethylene to propene, which was an important reaction in chemical industry. According to previous research, the catalytic conversion of 1-butene and ethylene to propene was a tandem reaction which involved isomerization of 1-butene to 2-butene and the subsequent cross metathesis between 2-butene and ethylene to propene [2]. Besides, several side reactions coexisted, such as isomerization of 1-butene to isobutene, and oligomerization of light olefins to high molecular weight compounds. The high acidity of catalyst stimulated these unwanted side-reactions, resulting in poor catalytic performance [40]. In this work, the main products were propene and 2-butene, and only slight amount of isobutene was detected as present in Table S2, since the weak acidic feature of catalysts. Therefore, the reaction could be described as shown in Scheme 1.

The effect of Si/Mo ratio on 1-butene conversion and propene selectivity was studied and shown in Fig. 9. Pure KIT-5 showed negligible conversion of 1-butene with no propene generation (not shown here). As Mo was introduced, all Mo-KIT-5 catalysts exhibited significant conversion of 1-butene and propene production. With the Si/Mo ratio decreased from 60 (Mo-KIT-5-60) to 45 (Mo-KIT-5-45), 1-butene conversion increased from 73.9 to 77.5%. Further reducing the Si/Mo ratio to 25, a slight decline of initial activity (about 4.1%) was observed for Mo-KIT-5-25 catalyst compared with Mo-KIT-5-40. However, the 1-butene conversion and propene selectivity began to decline significantly when the Si/Mo ratio was lower than 25, and 1-butene conversion and propene selectivity were as low as 50.6 and 56.1%, respectively for Mo-KIT-5-5 catalyst.

It was believed that a lower oxidation state of Mo and high dispersion of surface Mo species was beneficial for the olefin metathesis, since considerable amount of metal carbone species could be generated [41,42], which was the prerequisite of the reaction according to the well-known carbene-metallacycle mechanism [43]. The dispersion of surface Mo species was close connected with Mo content. At low Mo loading, the decrease of Si/Mo ratio led to the improvement of surface Mo species density. Thus, Mo-KIT-5-45 exhibited better catalytic performance than that of Mo-KIT-5-60. However, further decreasing Si/Mo ratio resulted in significantly declined BET surface area, which was against the dispersion of Mo species. Besides, as the Si/Mo ratio reduced, bulk MoO_3 began to appear as confirm by TEM (Fig. 3f) and XRD (Fig. 4g) results. Crystalline MoO_3 was believed to be inactive for olefin metathesis [7]. These explained the loss of catalytic activity for Mo-KIT-5-15 and Mo-KIT-5-5 catalysts with low Si/Mo ratios.

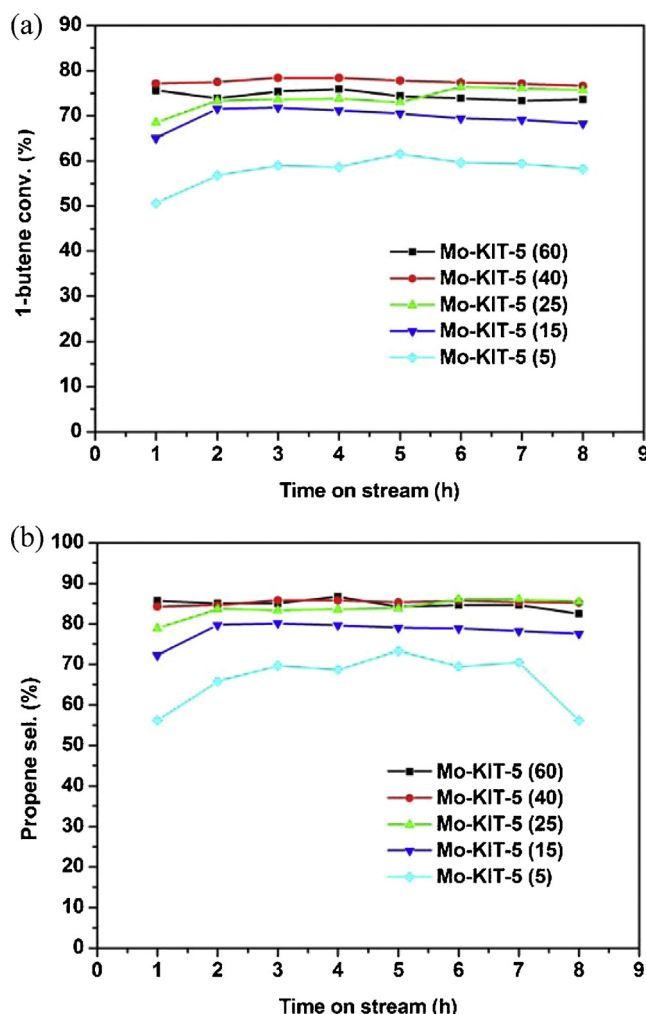


Fig. 9. 1-Butene conversions (a) and propene selectivities (b) versus time on stream over various Mo-KIT-5 catalysts. Reaction conditions: catalyst weight = 1.0 g; $T = 450^\circ\text{C}$; $P = 0.1 \text{ MPa}$; WHSV = 0.8 h^{-1} ; $\text{C}_2\text{H}_4/\text{C}_4\text{H}_8 = 2$.

The catalytic performance of one-pot hydrothermal synthesized Mo-KIT-5-40 catalyst was compared with supported Mo/KIT-5-40 and conventional Mo/SiO₂-40 catalysts with identical Mo loading prepared by impregnation method, as shown in Fig. 10. Conventional silica supported Mo/SiO₂-40 showed poor catalytic performance with 1-butene conversion of 52.2% and propene selectivity of 54.4% at steady-state. Supported Mo/KIT-5-40 exhibited higher initial 1-butene conversion (60.7%) and propene selectivity (71.3%) than those of Mo/SiO₂-40. But the activity gradually declined to the same level of Mo/SiO₂-40 after 8 h of reaction. In contrast, the 1-butene conversion and propene selectivity of one pot synthesized Mo-KIT-5-40 was as high as 77.5 and 84.5%, respectively, and the catalyst was quite stable. The excellent catalytic performance of Mo-KIT-5-40 was ascribed to its superior textural property since the larger BET surface area of Mo-KIT-5-40 could lead to a higher dispersion of Mo species, facilitating the metathesis reaction.

The catalytic performance of Mo-KIT-5 was also compared with other mesoporous Mo-containing silica material with same Mo content (2.5 wt%), namely Mo-SBA-15 with two-dimensional (2D) hexagonal arrangement of cylindrical pores and Mo-KIT-6 with 3D cylindrical pores (Fig. 11). As can be seen from Fig. 11, Mo-KIT-5 exhibited superior catalytic activity to control Mo-SBA-15 and Mo-KIT-6 catalysts. It was inferred that three dimensional cage type porous networks with a high surface area was beneficial for the high

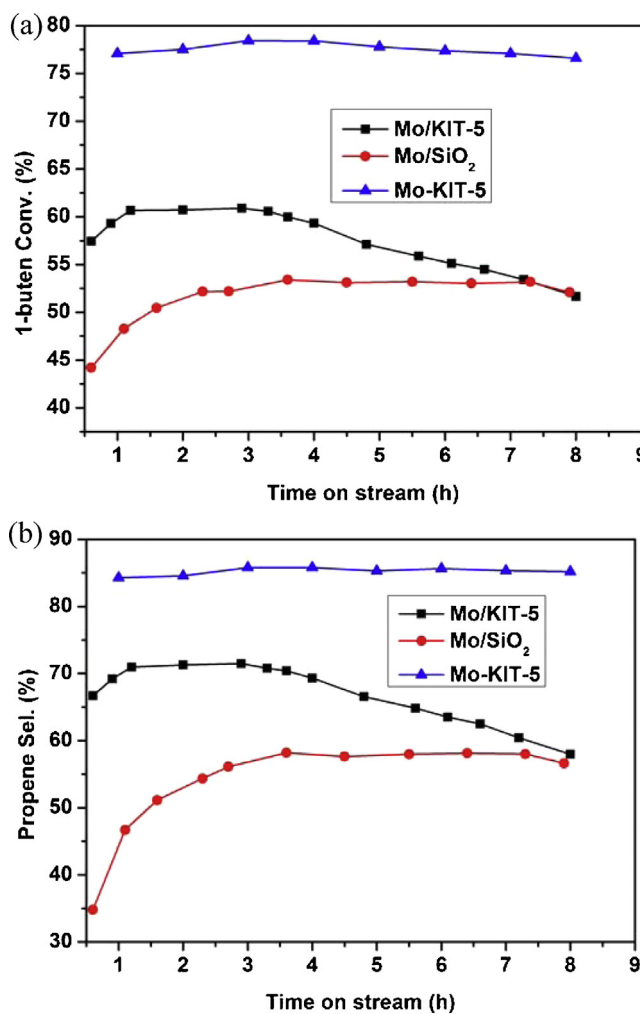


Fig. 10. 1-Butene conversions (a) and propene selectivities (b) versus time on stream over Mo-KIT-5-40, Mo/KIT-5-40 and Mo/SiO₂-40 catalysts. Reaction conditions: catalyst weight = 1.0 g; $T = 450^\circ\text{C}$; $P = 0.1 \text{ MPa}$; WHSV = 0.8 h^{-1} ; $\text{C}_2\text{H}_4/\text{C}_4\text{H}_8 = 2$.

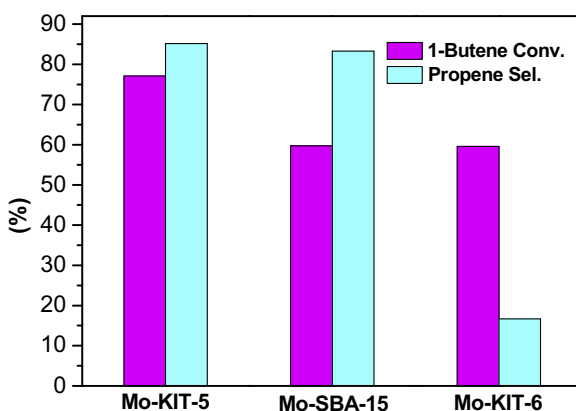


Fig. 11. Comparison of catalytic performances of different Mo containing mesoporous silica catalysts. Reaction conditions: catalyst weight = 1.0 g; $T = 450^\circ\text{C}$; $P = 0.1 \text{ MPa}$; WHSV = 0.8 h^{-1} ; $\text{C}_2\text{H}_4/\text{C}_4\text{H}_8 = 2$.

dispersion of Mo species, implementing the excellent metathesis activity. Besides, the 3D mesopores also facilitated transportation of reactants and products.

4. Conclusions

Various three-dimensional cage-like molybdenum containing mesoporous KIT-5 (Mo-KIT-5) catalysts with different Si/Mo ratios were prepared by one-pot hydrothermal synthesis and systematically characterized by multiple characterization techniques. It was found that the ordered mesoporous structure of KIT-5 could be retained after incorporation of Mo, even though the Si/Mo ratio as low as 15, as evident from TEM and N₂ physisorption analysis. However, further decreasing Si/Mo ratio to 5 resulted in collapse of mesoporous structure and the formation of bulk MoO₃ as suggested by XRD result. XPS result suggested that Mo was successfully incorporated into the KIT-5 framework and sample composed of both Mo⁶⁺ and Mo⁵⁺ species. NH₃-TPD analysis illustrated that Mo-KIT-5 samples contained weak acid sites. The Mo-containing catalysts were applied in catalytic conversion of 1-butene and ethylene to propene. With the decrease of Si/Mo ratio, the 1-butene conversion of Mo-KIT-5 first increased due to more active molybdenum oxides species generated, and then declined because of the destroy of mesoporous structure and formation of inactive bulk MoO₃. Mo-KIT-5-40 exhibited an improved catalytic performance compared with control supported Mo/KIT-5-40 and Mo/SiO₂-40 catalysts due to high dispersion of active Mo species. Moreover, Mo-KIT-5 also exhibited superior catalytic activity to Mo-SBA-15 and Mo-KIT-6 catalysts, suggesting that this kind of 3D cage type materials was very promising for catalytic conversion of 1-butene and ethylene to propene and could be applied in other heterogeneous catalytic reactions.

Acknowledgments

The authors are grateful for the financial support from the National Natural Science Foundation of China (Grant Nos. 21471086, 51572272), Natural Science Foundation of Ningbo (Grant No. 2015A610052), the Social Development Foundation of Ningbo (No. 2014C50013), and the K.C. Wong Magna Fund in Ningbo University.

Appendix A. Supplementary data

Supplementary data associated with this article can be found, in the online version, at <http://dx.doi.org/10.1016/j.molcata.2016.02.019>.

References

- [1] M. Stöcker, Microporous Mesoporous Mater. 29 (1999) 3–48.
- [2] J.C. Mol, J. Mol. Catal. A 213 (2004) 39–45.
- [3] R.L. Banks, G.C. Bailey, Ind. Eng. Chem. Prod. Res. Dev. 3 (1964) 170–173.
- [4] J.C. Mol, Catal. Today 51 (1999) 289–299.
- [5] T. Yamaguchi, Y. Tanaka, K. Tanabe, J. Catal. 65 (1980) 442–447.
- [6] R.H. Grubbs, S.J. Swetnick, J. Mol. Catal. 8 (1980) 25–36.
- [7] P. Topka, H. Balcar, J. Rathouský, N. Žilková, F. Verpoort, J. Čejka, Microporous Mesoporous Mater. 96 (2006) 44–54.
- [8] Y. Iwasawa, H. Ichinose, S. Ogasawara, M. Soma, J. Chem. Soc. Faraday Trans. I 77 (1981) 1763–1777.
- [9] Y. Wang, Q. Chen, W. Yang, Z. Xie, W. Xu, D. Huang, Appl. Catal. A 250 (2003) 25–37.
- [10] D. Zhang, X. Li, S. Liu, X. Zhu, F. Chen, L. Xu, Appl. Catal. A 472 (2014) 92–100.
- [11] S. Liu, X. Li, W. Xin, S. Xie, P. Zeng, L. Zhang, L. Xu, J. Nat. Gas Chem. 19 (2010) 482–486.
- [12] D.P. Debecker, M. Stoyanova, U. Rodemerck, F. Colbeau-Justin, C. Boissere, A. Chaumonnot, A. Bonduelle, C. Sanchez, Appl. Catal. A 470 (2014) 458–466.
- [13] H. Balcar, J. Čejka, Coord. Chem. Rev. 257 (2013) 3107–3124.
- [14] T.I. Bhuiyan, P. Arudra, M.N. Akhtar, A.M. Aitani, R.H. Abudawoud, M.A. Al-Yami, S.S. Al-Khattaf, Appl. Catal. A 467 (2013) 224–234.
- [15] C. Lin, K. Tao, H.B. Yu, D.Y. Hua, S.H. Zhou, Catal. Sci. Techn. 4 (2014) 4010–4019.
- [16] H. Balcar, D. Mishra, E. Marceau, X. Carrier, N. Žilková, Z. Bastl, Appl. Catal. A 359 (2009) 129–135.
- [17] T. Ookoshi, M. Onaka, Chem. Commun. (1998) 2399–2400.
- [18] B. Hu, H. Liu, K. Tao, C. Xiong, S. Zhou, J. Phys. Chem. C 117 (2013) 26385–26395.

- [19] J. Čejka, *Appl. Catal. A* 254 (2003) 327–338.
- [20] K. Bouchmella, P. Hubert Mutin, M. Stoyanova, C. Poleunis, P. Eloy, U. Rodemerck, E.M. Gaigneaux, D.P. Debecker, *J. Catal.* 301 (2013) 233–241.
- [21] D.P. Debecker, K. Bouchmella, M. Stoyanova, U. Rodemerck, E.M. Gaigneaux, P. Hubert Mutin, *Catal. Sci. Tech.* 2 (2012) 1157–1164.
- [22] F. Kleitz, D. Liu, G.M. Anilkumar, I.-S. Park, L.A. Solovyov, A.N. Shmakov, R. Ryoo, *J. Phys. Chem. B* 107 (2003) 14296–14300.
- [23] P. Srinivasu, S. Alam, V.V. Balasubramanian, S. Velmathi, D.P. Sawant, W. Böhlmann, S.P. Mirajkar, K. Ariga, S.B. Halligudi, A. Vinu, *Adv. Funct. Mater.* 18 (2008) 640–651.
- [24] C. Anand, S.V. Priya, G. Lawrence, D.S. Dhawale, S. Varghese, M.A. Wahab, K.S. Prasad, A. Vinu, *Catal. Today* 204 (2013) 125–131.
- [25] C. Anand, P. Srinivasu, G.P. Mane, S.N. Talapaneni, M.R. Benzigar, S. Vishnu Priya, S.S. Al-deyab, Y. Sugi, A. Vinu, *Microporous Mesoporous Mater.* 167 (2013) 146–154.
- [26] D. Shobha, M.A. Chari, S.T. Selvan, H. Oveisi, A. Mano, K. Mukkanti, A. Vinu, *Microporous Mesoporous Mater.* 129 (2010) 112–117.
- [27] A. Ramanathan, R. Maheswari, B.P. Grady, D.S. Moore, D.H. Barich, B. Subramaniam, *Microporous Mesoporous Mater.* 175 (2013) 43–49.
- [28] A. Ramanathan, H. Zhu, R. Maheswari, B. Subramaniam, *Chem. Eng. J.* 278 (2015) 113–121.
- [29] V.V. Balasubramanian, P. Srinivasu, C. Anand, R.R. Pal, K. Ariga, S. Velmathi, S. Alam, A. Vinu, *Microporous Mesoporous Mater.* 114 (2008) 303–311.
- [30] K. Tao, L. Shi, Q. Ma, D. Wang, C. Zeng, C. Kong, M. Wu, L. Chen, S. Zhou, Y. Hu, N. Tsubaki, *Chem. Eng. J.* 221 (2013) 25–31.
- [31] G.M.S. El Shafei, M.M. Mokhtar, *Colloids Surf. A* 94 (1995) 267–277.
- [32] M.A. Villegas, J.M.F. Navarro, J. Mater. Sci. 23 (1988) 4503–4512.
- [33] S. Daniele, M.N. Ghazzal, L.G. Hubert-Pfalzgraf, C. Duchamp, C. Guillard, G. Ledoux, *Mater. Res. Bull.* 41 (2006) 2210–2218.
- [34] Y. Liu, X. Ma, S. Wang, J. Gong, *Appl. Catal. B* 77 (2007) 125–134.
- [35] A. Ramanathan, B. Subramaniam, R. Maheswari, U. Hanefeld, *Microporous Mesoporous Mater.* 167 (2013) 207–212.
- [36] A. Duan, G. Wan, Z. Zhao, C. Xu, Y. Zheng, Y. Zhang, T. Dou, X. Bao, K. Chung, *Catal. Today* 119 (2007) 13–18.
- [37] T. Kataoka, J.A. Dumesic, *J. Catal.* 112 (1988) 66–79.
- [38] L. Vordonis, P.G. Koutsoukos, A. Lycurghiotis, *Colloids Surf.* 50 (1990) 353–361.
- [39] L. Vordonis, P.G. Koutsoukos, A. Lycurghiotis, *J. Catal.* 98 (1986) 296–307.
- [40] H. Liu, K. Tao, P. Zhang, W. Xu, S. Zhou, *New J. Chem.* 39 (2015) 7971–7978.
- [41] K.J. Ivin, J. Mol. Olefin Metathesis and Metathesis Polymerization, Academic Press, New York, 1997.
- [42] B. Zhang, N. Liu, Q. Lin, D. Jin, *J. Mol. Catal.* 65 (1991) 15–28.
- [43] R.H. Grubbs, P.L. Burk, D.D. Carr, *J. Am. Chem. Soc.* 97 (1975) 3265–3267.